Journal of Colloid and Interface Science 589 (2021) 356–366

Contents lists available at ScienceDirect

Journal of Colloid and Interface Science

journal homepage: www.elsevier.com/locate/jcis

Regular Article

Dynamics of long-term protein aggregation on low-fouling surfaces

Mohammadhasan Hedayati [a], Diego Krapf [b,c,d,*], Matt J. Kipper [a,b,c,*]

[a] Department of Chemical and Biological Engineering, Colorado State University, Fort Collins, CO 80523, USA
[b] School of Biomedical Engineering, Colorado State University, Fort Collins, CO 80523, USA
[c] School of Advanced Materials Discovery, Colorado State University, Fort Collins, CO 80523, USA
[d] Department of Electrical and Computer Engineering, Colorado State University, Fort Collins, CO 80523, USA

GRAPHICAL ABSTRACT

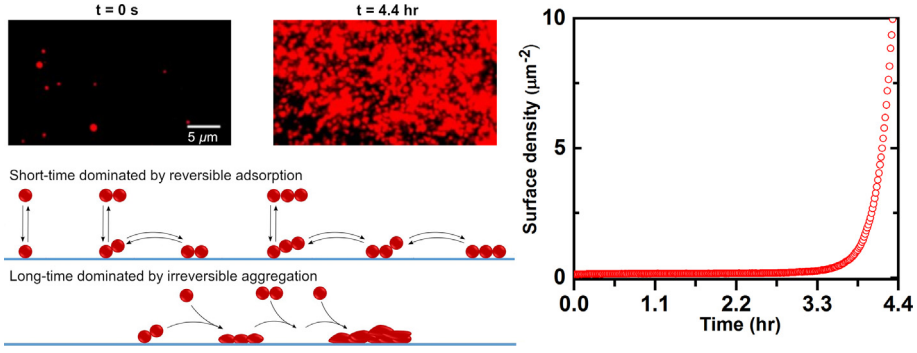

ARTICLE INFO

Article history:
Received 28 October 2020
Revised 13 December 2020
Accepted 1 January 2021
Available online 08 January 2021

Keywords:
Protein adsorption
Oligomerization
PEG
Polyelectrolyte multilayer
Polyelectrolyte complex nanoparticle
Single-molecule microscopy

ABSTRACT

Understanding the mechanisms of protein interactions with solid surfaces is critical to predict how proteins affect the performance of materials in biological environments. Low-fouling and ultra-low fouling surfaces are often evaluated in short-term protein adsorption experiments, where 'short-term' is defined as the time required to reach an initial apparent or pseudo-equilibrium, which is usually less than 600 s. However, it has long been recognized that these short-term observations fail to predict protein adsorption behavior in the long-term, characterized by irreversible accumulation of protein on the surface. This important long-term behavior is frequently ignored or attributed to slow changes in surface chemistry over time—such as oxidation—often with little or no experimental evidence. Here, we report experiments measuring protein adsorption on "low-fouling" and "ultralow-fouling" surfaces using single-molecule localization microscopy to directly probe protein adsorption and desorption. The experiments detect protein adsorption for thousands of seconds, enabling direct observation of both short-term (reversible adsorption) and long-term (irreversible adsorption leading to accumulation) protein-surface interactions. By bridging the gap between these two time scales in a single experiment, this work enables us to develop a single mathematical model that predicts behavior in both temporal regimes. The experimental data in combination with the resulting model provide several important insights: (1) short-term measurements of protein adsorption using ensemble-averaging methods may not be sufficient for designing antifouling materials; (2) all investigated surfaces eventually foul when in long-term contact with protein solutions; (3) fouling can occur through surface-induced oligomerization of proteins which may be a distinct step from irreversible adsorption; and (4) surfaces can be designed to reduce oligomerization or the adsorption of oligomers, to prevent or delay fouling.

* Corresponding authors.
E-mail addresses: Diego.Krapf@colostate.edu (D. Krapf), mkipper@colostate.edu (M.J. Kipper).

https://doi.org/10.1016/j.jcis.2021.01.001
0021-9797/

1. Introduction

Understanding nonspecific protein adsorption mechanisms at solid-liquid interfaces is critical for rational design of surfaces for biomedical and industrial applications such as medical devices, drug delivery carriers, marine coatings, and biosensors [1–4]. For blood-contacting medical devices for example, non-specific plasma protein adsorption occurs when surfaces come into contact with blood [4]. This is the first step of subsequent adverse biological responses such as coagulation, thrombosis, and infection that leads to reduced device efficacy and functionality, and sometimes to device failure. Therefore, experimental and theoretical descriptions of protein adsorption kinetics can enable improved design of surfaces that resist nonspecific protein adsorption.

Protein interactions with biomaterial surfaces occur through electrostatic phenomena, van der Waals forces, hydrogen bonds, and hydrophobic dehydration [5]. These protein-surface interactions can result in reversible or irreversible binding, and some proteins may also undergo conformational changes and aggregation after adsorption. Approaches to design protein-resistant biomaterials are primarily based on surface modifications that reduce nonspecific protein adsorption by controlling these protein-surface interactions [7,8]. Surface physical chemistry modification could be an efficient method for preventing or reducing protein adsorption, as long as the driving forces for protein adsorption can be minimized for long periods of time [1]. However, despite decades of efforts to improve protein resistance of biomaterials, there is no known synthetic material with absolute protein resistance in complex biological environments.

The resistance to protein adsorption of a new material or surface is frequently evaluated by experimental ensemble averaging methods such as quartz crystal microbalance (QCM) and surface plasmon resonance (SPR), to measure the amount of adsorbed protein, and by spectroscopic methods such as infrared spectroscopy and circular dichroism, to provide details of protein chemistry and structure. These methods can reveal important details about average physical and chemical changes that occur during or after protein adsorption [9]. Several low-fouling and ultralow-fouling materials such as polysaccharide-based polyelectrolyte multilayer (PEM) surfaces, glycosaminoglycan (GAG) coated surfaces, zwitterionic surfaces, and polyethylene glycol (PEG) brush surfaces have been reported, and their resistance to protein adsorption has been evaluated with these techniques in short-term experiments [10–15]. However, because interfacial dynamics and conformation of proteins cannot be observed with single-molecule resolution using ensemble-averaging methods, conclusions about the antifouling properties of surfaces may be overly simplified or even incorrect [16].

Protein adsorption experiments used to design and compare low-fouling and ultralow-fouling surfaces often focus on the kinetics of protein adsorption over relatively short time-scales (<30 min) [17]. These experiments, however, often fail to predict protein fouling that occurs when surfaces are exposed to protein solutions for longer periods of time. PEG brushes and other polymer brush chemistries, for example, may exhibit long-term fouling due to changes in the surface chemistry upon exposure to biological environments, or environments that present thermal or oxidative challenges, which could be found in many applications [18–21].

Single-molecule microscopy has significant advantages with respect to characterizing protein-surface interactions that involve interfacial dynamics to elucidate complex mechanistic details [22–24]. In particular, by using total internal reflection fluorescence (TIRF) microscopy, a large number of protein molecules can be tracked in real time to measure phenomena such as adsorption, desorption, binding, and surface diffusion. Studies using single-molecule localization microscopy have revealed how interactions of protein with nanostructured surfaces are affected by surface structure and chemistry as well as protein properties [25–31]. The adsorption and relaxation kinetics of bovine serum albumin (BSA) and fibrinogen on uncharged surfaces with different hydrophobicity were investigated under flow conditions [32]. Kinetics analysis revealed a constant spreading rate, which increased with substrate hydrophobicity. Recently, we characterized the kinetics of BSA on low-fouling surfaces using single-molecule localization microscopy [24]. We found that the desorption rate of proteins from the surface was not constant, a result that was explained in terms of proteins forming oligomers in solution, where each oligomer has unique kinetic parameters. These studies highlight the utility of single-molecule microscopy to uncover the complex mechanistic details underlying protein-surface interactions.

Several mathematical models have been proposed to explain experimental observations of protein interactions with different surfaces [6,33–35]. The Langmuir adsorption model is one of the most basic models proposed for proteins that are assumed to behave like rigid particles on surfaces [36]. These particles reversibly adsorb to distinct surface sites and form one uniform layer without lateral interactions between the molecules that are already adsorbed under equilibrium conditions. The Langmuir adsorption model is frequently used to interpret short term (pseudo-)equilibrium experiments using techniques that measure the amount of adsorbed protein in real-time, such as SPR and QCM. The Langmuir model was improved by the random sequential adsorption (RSA) model which accounts for irreversible adsorption of proteins from the bulk solution to random available surface sites [37]. According to this model, pre-adsorbed proteins block further protein adsorption at designated sites. Further models were also proposed to account for spreading of proteins upon adsorption on solid surfaces [6]. The advantage of these models is that they can predict the irreversible conformational changes of some of the adsorbed proteins. Recent evidence shows that models that consider molecules that are further allowed to reversibly oligomerize in solution reveal anomalous kinetics. Such anomalous kinetics are characterized by individual molecules exhibiting surface dwell times with heavy tail distributions, *i.e.*, marked deviations from an exponential distribution [24,38]. In these models, particles adsorb to the surface, such that oligomers with different size have different desorption rates. Each of these studies has provided important insights into protein interactions on solid interfaces. However, all of these models have been developed either to explain observations from ensemble averaging techniques or short-term studies, thus they do not make predictions about long-term behavior.

In this work, we use single-molecule TIRF microscopy to investigate the dynamics of protein interactions with various biomaterial surfaces that were previously characterized and considered as low-fouling or ultralow-fouling materials, based on short-term equilibrium protein binding experiments [16,39]. Some of these ultralow-fouling surfaces have been proposed for reducing protein adsorption in blood-contacting applications [39]. We study the mechanism of surface interactions with two important blood proteins—albumin and fibrinogen. In particular, we investigate long-term protein interactions to elucidate the mechanism of protein adsorption using single-molecule microscopy experiments. Here, long-term is defined as the time required to observe accumulation and aggregation of proteins. These long-term experiments range from less than 1 h to over 3 h, depending upon the surface and protein pair. On all of the surfaces studied, two limiting regimes of protein interactions are observed. In the short term, surface-protein interactions are governed by reversible adsorption and desorption, and they are characterized by low surface concentrations. However, long-term experiments reveal a regime characterized by a delayed increase in protein adsorption rate. To better

understand this phenomenon, we propose a mathematical model for protein interactions with low-fouling or ultralow-fouling interfaces that accurately describes the long-term behavior. In particular, the model includes the possibility of reversible oligomerizaton in solution and surface-induced irreversible aggregation effects. Because this new model is competent to describe the long-term fouling of otherwise low- or ultralow-fouling surfaces, it can be adopted to optimize ultralow-fouling surfaces for long-term blood-contacting applications. To the best of our knowledge, this behavior has not been reported by any proposed models in the literature. This new model may also be expanded for other surfaces used in food production, medical materials, and marine applications.

2. Materials and methods

2.1. Materials

Chitosan (CHI) was purchased from Heppe Medical Chitosan (Mw = 80–200 kDa, degree of deacetylation >92%). Chondroitin sulfate sodium (CS) salt (from shark cartilage, 6% sulfur, 6-sulfate/4-sulfate = 1.24, Mw = 84.3 kDa), hyaluronic acid (HA) sodium salt (Mw = 743 kDa), sodium acetate, β-mercaptoethanol, catalase from bovine liver, and glucose oxidase were purchased from Sigma Aldrich. Heparin sodium (HEP) (from porcine intestinal mucosa, 12.5% sulfur) was purchased from Celsus Laboratories. 2-[Methoxy(polyethyleneoxy)$_{6-9}$ propyl]trimethoxysilane was purchased from Gelest. Anhydrous toluene was purchased from MilliporeSigma. Glacial acetic acid and ethanol (200 proof 99.5 + %) were purchased from Acros Organics. BSA conjugated to Alexa Fluor 647 and fibrinogen (FIB) from human plasma conjugated to Alexa Fluor 647 were purchased from Thermo Fisher Scientific. All the reagents were used as received. A Millipore water purification unit was used to obtain 18.2 MΩ cm water, used for making all aqueous solutions.

2.2. Preparation of PEG brush surfaces

PEG brush surfaces were constructed with a grafting-to approach, as previously described [24]. Prior to functionalization, the fused silica wafers were thoroughly washed with acetone, ethanol, and deionized water and dried with ultrapure N_2. Wafers were then exposed to oxygen plasma under vacuum for 10 min to form hydroxyl (—OH) groups on the surface. The substrates were subsequently incubated in 1% v/v PEG silane (2-[methoxy (polyethyleneoxy)$_{6-9}$ propyl]trimethoxysilane) dissolved in anhydrous toluene [40,41]. The reaction was performed at room temperature with incubation times of 20 min and 60 min, to construct PEG surfaces with low (PEG_{lg}) and high (PEG_{hg}) grafting density, respectively. Finally, surfaces were rinsed multiple times with toluene and deionized water and dried with ultrapure N_2.

2.3. Grafting density determination for PEG brush surfaces

The thickness of the dry PEG brush was measured by ellipsometry using a J.A. Woollam VASE variable angle spectroscopic ellipsometer and data analysis was done using the J. A. Woollam WVASE32 software package. Each surface was spectrally scanned with an incident angle between 60° and 80°, in increments of 5°, over a wavelength range from 500 nm to 900 nm. The collected spectra were fit to a three-layer planar model of the solid surface, which accounts for the refractive index of air (n = 1.003), PEG (n = 1.43), silicon oxide layer (n = 1.457), and silicon (n = 3.881). Dry thicknesses were measured on triplicate samples for each condition. The dry PEG brush thickness (h_{dry}) was related to grafting density σ via the relation $\sigma = \rho_{dry} h_{dry} N_A / M_w$ where ρ_{dry} is the dry density of the PEG monomer repeat unit, N_A is Avogadro's number, and M_w is the average molecular weight of the PEG polymer [1]. The resulting grafting density for PEG_{lg} and PEG_{hg} is 0.15 ± 0.06 and 0.32 ± 0.03 chains/nm^2, respectively.

2.4. Preparation of PEM surface

Polysaccharide solutions were prepared in 0.2 M sodium acetate and acetic acid at pH 5.0. Chitosan (1.33 mg mL^{-1}) and hyaluronan (0.5 mg mL^{-1}) solutions were prepared by stirring for 2 h at room temperature. Solutions were clarified by filtration through 0.22 μm syringe filters. PEM samples were prepared on glass-bottom Petri dishes (50 mm Pelco Petri dishes, Willco Wells, Amsterdam) as previously described [39,42,43]. Briefly, Petri dishes were first treated with oxygen plasma for 10 min, to ensure a clean, oxidized surface. PEMs were constructed with CHI as the polycation and HA as the polyanion. First, the oxidized surface was exposed to an acidified water rinse (pH 4.0, acidified with acetic acid), for 6 min. The layer-by-layer process was conducted by exposing solutions to the surface in the following sequence: polycation (CHI), rinse, polyanion (HA), rinse; each one for 6 min. The sequence was repeated until a 19-layer PEM (terminating with CHI) had been adsorbed.

2.5. Preparation of glycocalyx-mimetic surfaces (PEM+PCNs)

Polyelectrolyte complex nanoparticles (PCNs) containing CHI and GAGs (CS or HEP) were formed, as previously described [43–45]. After the layer-by-layer assembly of 19-layer CHI-HA PEMs, either CS-CHI PCNs or HEP-CHI PCNs were adsorbed [39,44]. The resulting samples are referred to as PEM+PCNs (CS-CHI) and PEM +PCNs (HEP-CHI). The time of the adsorption steps was doubled to 12 min for the PCNs adsorption, followed by a final rinse with acidified water, as previously described [44].

2.6. Total internal reflection fluorescence (TIRF) microscopy

Total internal reflection fluorescence (TIRF) microscopy was carried out for single-molecule tracking experiments. The microscope was home built around an Olympus IX71 body with a 640-nm laser line as excitation source (DL640-150-O, CrystaLaser). The laser was directed into a 100× objective lens (Olympus PlanApo, NA = 1.45) and fluorescence images were acquired with a back-illuminated EMCCD camera (Andor iXon DU-888) operated at −70 °C and electronic gain of 60 [46,47]. To maintain constant focus during the whole imaging time, we employed an autofocus system (CRISP, Applied Scientific Instrumentation) in combination with a piezoelectric stage (Z-100, Mad City Labs). For excitation, an optical density filter with ND = 1.5 was used in the laser path and an incident angle above the critical angle was employed to achieve total internal reflection. Emission was collected through a Semrock bandpass filter.

To reduce photobleaching, an enzymatic oxygen scavenger system was used in the imaging buffer. The imaging buffer for screening protein adsorption and desorption consisted of 50 mM Tris−HCl (pH 8.0), 10 mM NaCl, 0.8% glucose, 0.15 mg mL^{-1} glucose oxidase, 34 μg mL^{-1} catalase, and 1% β-mercaptoethanol [48]. A perfusion chamber of 9 mm in diameter and 0.8 mm in depth containing the synthetic surface was filled with the protein solution and time-lapse imaging was started right away. Imaging was performed whereby an image was obtained every 2 s over a total period of the experiment. Exposure time in each frame was limited to 90 ms using a Uniblitz high-speed optical shutter syn-

chronized with the camera acquisition. During imaging, there was always protein present in the bulk solution.

Albumin and fibrinogen interactions with PEG brush surfaces, PEM, and PEM+PCNs were directly measured via tracking of at least 10^4 individual protein molecules in single-molecule experiments. Dilute concentrations of protein were used for each protein-surface pair (see Table S.1). Protein concentrations were all optimized, so that during the first 10 min of imaging, the surface protein concentration is less than 0.2 μm^{-2}, thereby enabling single-particle tracking. Time-lapse imaging continued until the field of view was covered with the protein. This condition still indicates very low surface coverage, as the size of an adsorbed protein is much smaller than the size of a pixel in the image. During the experiments, the perfusion chamber was sealed to prevent evaporation and keep a constant solution volume.

2.7. Image processing and single-molecule tracking

Images were acquired using Andor IQ 2.3 software and saved as 16-bit tiff files. Images were filtered using a Gaussian kernel with a standard deviation of 1.0 pixel in ImageJ. Single-particle tracking of BSA and FIB was performed in MATLAB using the U-track algorithm under thorough manual inspection of detection and tracking [49]. Particles detected in consecutive frames within 2 pixels (260 nm) were linked in order to determine the persistence of a protein on the surface. When the surface protein density is low, individual protein molecules can be resolved. This enables us to directly observe several tens of thousands of individual adsorption and desorption events in the field of view in a single experiment. As the protein density increases, individual protein molecules can no longer be resolved. Instead, the total protein adsorbed per area is determined from the intensity integrated over the surface area of the image, where the intensity per protein molecule is obtained from the intensity extrapolated to the low-protein number limit.

3. Results and discussion

To accurately quantify protein interactions on low fouling surfaces, we selected PEG brush surfaces (Fig. 1(a)) and imaged individual fluorescently labeled albumin by TIRF microscopy. A low concentration (5 nM) of protein molecules in imaging buffer was used to enable single-molecule detection as proteins adsorb to and desorb from the solid–liquid interface. Fig. 1(c) shows the surface density of fluorescently labeled albumin as a function of time on three different replicates of PEG with low grafting density (PEG_{lg}) along with representative individual microscopy frames of labeled proteins on the surface at three time points. The kinetics of protein adsorption to the PEG_{lg} surfaces exhibits two different asymptotic behaviors. At short times, individual molecules reversibly adsorb to and desorb from the surface. Kinetics governed by reversible adsorption and desorption persists for an extended period of time that depends on surface density and bulk protein concentration. A thorough characterization of this regime for BSA kinetics was recently reported by us [24] showing non-trivial behavior due to reversible dimerization of proteins in solution. Typically, short-term experiments reveal this type of reversible adsorption/desorption behavior. However, Fig. 1(c) reveals a sharp increase in surface density at longer times.

To characterize the adsorption, desorption, and aggregation behavior of albumin on the low-fouling surfaces over the full time-scale of the experiment, we develop a mathematical model that quantifies the kinetics of surface-protein interactions. We have recently shown that short-time desorption of albumin from low-fouling surfaces involves multiple species related to oligomers of different sizes [24]. As a consequence, each multimer has a desorption rate that depends on the number of monomers, and anomalous desorption kinetics are observed. In addition, over the timescale of our experiments, the solution is in equilibrium and irreversible aggregation is not observed in the liquid solution, as the hydrodynamic radius of the BSA does not change [24]. This result suggests the irreversible oligomerization is surface-induced. The short-time behavior in our single-molecule experiments shown in Fig. 1(c) can be described by a linear model of adsorption of non-interacting species (*e.g.*, a Langmuir model [33,36]). In our model, we assume first-order, reversible adsorption without limitation on the number of surface sites or the amount of protein in solution. However, this reversible adsorption does not dominate the behavior indefinitely. The long-time behavior resembles nucleated self-assembly mechanisms, such as those associated with amyloid fibril formation [50–53]. Here we propose a surface-mediated nucleation model (Scheme 1).

In our model, we denote the state of a protein in an oligomer as $p_{i,j}$, where i indicates the number of protein monomers in the oligomer, and $0 \leq j \leq i$ is the number of monomers in the oligomer that are adsorbed on the surface. For example, $p_{3,2}$ is the (surface) concentration of trimers with two monomers bound to the surface

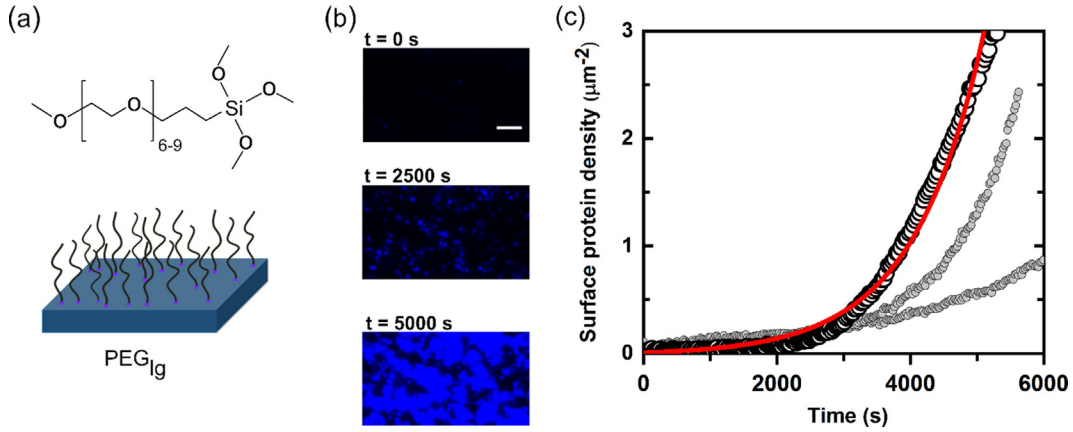

Fig. 1. (a) Chemical structure of the PEG-silane used to prepare PEG brush surfaces along with a sketch of low grafting PEG brush surface. (b) Representative TIRF micrographs during BSA adsorption experiments on PEG_{lg} at different time scales, scale bar = 5 μm. (c) BSA surface density as a function of time for three replicates. The black thick circles correspond to the TIRF micrographs in (b), and the red solid line represents the proposed model fit to the black curve. (For interpretation of the references to colour in this figure legend, the reader is referred to the web version of this article.)

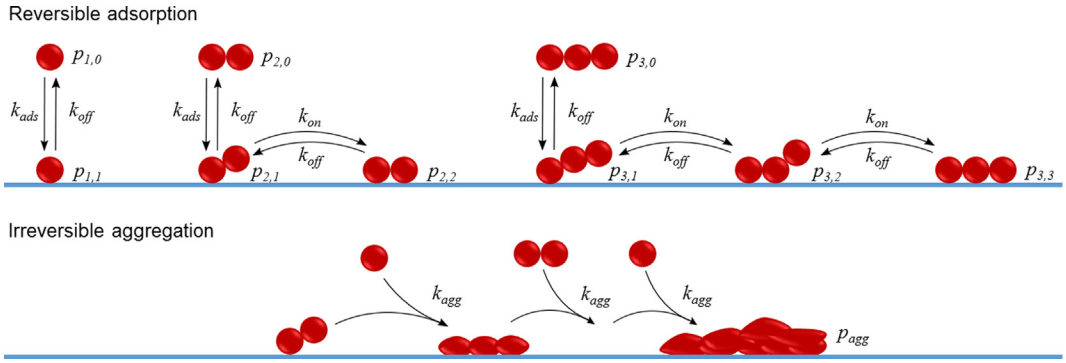

Scheme 1. Conceptual representation of our model for reversible adsorption and desorption of protein oligomers and irreversible aggregation.

and $p_{i,0}$ is the (solution) concentration particles in state $(i,0)$, that is oligomers of i monomers that are not bound to the surface (free in solution). For each sized oligomer, there are multiple adsorbed states, as shown in Scheme 1. We assume that oligomer desorption from the surface occurs as a series of elementary reactions, *e.g.*, a trimer completely bound to the surface desorbs first one of its monomers, then the second, and at last the third one, to become a free trimer in solution. Therefore, the desorption of smaller oligomers is much faster than the desorption of larger oligomers, and the distribution of oligomer sizes for adsorbed particles evolves over time. However, this fully reversible model does not include the long-term aggregation observed in Fig. 1.

To describe the long-time behavior, we include in the kinetic model a rate of irreversible, surface-mediated aggregation, whereby any protein monomer in a surface-adsorbed oligomer can aggregate with a particle in a dissolved oligomer to form a higher adsorbed oligomer, also shown in Scheme 1. Namely, our model includes reversible reactions of the form

$$p_{i,0} \underset{k_{off}}{\overset{k_{ads}}{\rightleftharpoons}} p_{i,1} \underset{k_{off}}{\overset{k_{on}}{\rightleftharpoons}} p_{i,2} \tag{1}$$

and irreversible reactions of the form

$$p_{i,j} + p_{l,0} \overset{k_{agg}}{\rightarrow} p_{i+l,j}, \tag{2}$$

where k_{ads} is the adsorption rate coefficient from the bulk solution, k_{on} and k_{off} are adsorption and desorption rate coefficients of monomers within a particle that is bound to the surface, respectively, and k_{agg} is the (irreversible) aggregation rate. The specific interactions described by these rate coefficients depend upon the protein-surface pair. For example, on polar or charged surfaces, protein adsorption occurs when a surface-bound water molecule or ion is exchanged for a polar or charged group on the protein surface. This step is often reversible with a small enthalpy change. These interactions are favored by the increase in entropy associated with the release of water and/or ions from the surface in exchange for a protein. The density and strength of these interactions depends upon the chemical details of both the protein and the surface. In contrast, the surface confinement of bound protein catalyzes irreversible oligomerization with proteins from solution, described by k_{agg}. This reaction could involve the sum of multiple elementary steps (*e.g.*, collision, rearrangement, accumulation of protein-protein interactions, and protein denaturation) that are lumped here into a single k_{agg}.

Next, we cast these reactions into a set of ordinary differential equations. When a particle of i monomers adsorbs from the solution to the surface it turns into state $(i,1)$ and the Eqs. (1) and (2) lead to the differential equation for $p_{i,1}$,

$$\frac{dp_{i,1}}{dt} = k_{off}\left[2p_{i,2} - p_{i,1}\right] + k_{ads}p_{i,0} - (i-1)k_{on}p_{i,1} + k_{agg}\left[\sum_{l=1}^{i-1}(i-l)(p_{i-l,1})(p_{l,0}) - ip_{i,1}\sum_{l=1}^{\infty}p_{l,0}\right], \tag{3}$$

where the first three right-side terms represent reversible reactions and the last term is irreversible aggregation. In general, the differential equation for the probability of being in state (i,j) is

$$\frac{dp_{i,j}}{dt} = k_{off}\left[(j+1)p_{i,j+1} - jp_{i,j}\right] + k_{on}\left[(i-j+1)p_{i,j-1} - (i-j)p_{i,j}\right] + k_{agg}\left[\sum_{l=1}^{i-j}(i-l)(p_{i-l,j})(p_{l,0}) - ip_{i,j}\sum_{l=1}^{\infty}p_{l,0}\right], \tag{4}$$

for $1 \le j \le i$.

A key assumption to solve our model is that the concentration of different sized oligomers in solution does not change during the time of the experiments, *i.e.*, there is no depletion of proteins in the solution due to surface binding. As a consequence, all $p_{i,0}$ are treated as constants that are in thermodynamic equilibrium, as previously done [24].

For simplicity of implementation and in order to obtain a tractable solution, we make the approximation that oligomers of aggregation number $i \ge 4$ do not desorb. This assumption is based on the fact that large oligomers take a very long time to desorb. The robustness of this assumption can be directly tested. Thus, Eq. (4) is valid for $1 \le i \le 3$ and we introduce the notation p_{agg} for the density of monomers on the surface within an oligomer with $i \ge 4$. Within the approximation that no depletion from the solution occurs, the set of equations has finite dimensions and is linear. Thus, it can be solved analytically for the population of each component as a function of time. The rate equation for p_{agg} is

$$\frac{dp_{agg}}{dt} = (i+l)k_{agg}\sum_{i=1}^{\infty} i\left[\sum_{j=1}^{i} p_{i,j}\left(\sum_{i=1}^{\infty} lp_{l,0}\right)\right] + k_{agg}p_{agg}\sum_{l=1}^{\infty} lp_{l,0}. \tag{5}$$

In the single-molecule detection by TIRF microscopy, we can observe the total intensity on the surface, which is proportional to the total amount of protein adsorbed. The proportionality constant can be determined for each experiment, which enables the surface average intensity to be converted to surface protein concentration. Adsorption rate coefficients (k_{ads}) were determined during the short-time behavior, from single-molecule experiments and expressed as the total number of adsorption events relative to the elapsed time, the protein concentration in the solution, and the area of the field of view. Similarly, the rate coefficient for desorption (k_{off}) can be estimated from the rate at which single monomers

vanish from the surface from one frame to the next. The k_{off} was determined from survival probabilities of an individual monomer. Specifically,

$$s_1(\tau) = \int_{\tau}^{\infty} \varphi(t)dt = e^{-k_{off}\tau}, \quad (6)$$

where we denote s_1 as the survival probability for a monomer on the surface, and τ is the time since a particle initially adsorbed. Note that the survival probability for a surface oligomer of size n is $s_n(\tau) = e^{-k_n\tau}$ with $k_n = nk_{off}^n/k_{on}^{n-1}$ [24]. In practice, during single molecule experiments, the distribution of dwell times is usually obtained for particles of any size. However, the particles that are single monomers are statistically the fastest to desorb. Thus, it is possible to obtain k_{off} directly from the survival probability in the short-time limit $\tau \to 0$.

For BSA interacting with the PEG_{lg} surface, the measured k_{ads} and k_{off} parameters are 0.62 ± 0.14 s^{-1} μm^{-2} μM^{-1} and 0.1 ± 0.00 6 s^{-1}. Further, k_{agg} and K_{eq} parameters were adjusted so that the model matched the experimental data, where $K_{eq} = k_{on}/k_{off}$. The last adjustable parameter is the fraction that describes the distribution of monomers, dimers, and trimers in solution, which was determined based on our previously published results for albumin [24]. All of these adjustable parameters are reported in Table S.2. The proposed model captures the key features of the experimental data, as shown in Fig. 1.

The above-mentioned parameters affect the relative transition between the short- and long-term behavior, and the overall rate of protein aggregation on the surface. To illustrate this concept, model solutions were obtained for three different parameters (k_{ads}, K_{eq}, and k_{agg}) over orders of magnitude at constant protein concentration and fraction of monomer, dimer and trimer in the solution. Fig. 2 indicates that all three parameters can influence the transition time at which the irreversible aggregation begins to dominate the process. When the adsorption rate coefficient (k_{ads}) is decreased (Fig. 2(a)), the irreversible aggregation is delayed. We also studied the impact of equilibrium constant (K_{eq} = k_{on} / k_{off}) on the behavior of the proposed model (Fig. 2(b)). The model proposes that K_{eq} has a weaker effect on the shape of the model, but by increasing K_{eq} over orders of magnitude, the time at which irreversible adsorption begins to dominate can be altered, without changing the rate of aggregation. By increasing the rate of desorption (k_{off}) (decreasing K_{eq}), protein molecules have reduced dwell time on the surface, leading to less interactions between the protein and surface and less chance of denaturation or aggregation on the surface. The rate of aggregation (k_{agg}) has a stronger effect on the induction of irreversible aggregation (Fig. 2(c)). In particular, by slightly increasing k_{agg}, the aggregation phenomenon occurs dramatically faster, leading to higher protein density on the surface.

In order to demonstrate that the model is generally applicable, we prepared four different surfaces and performed single-molecule localization microscopy to study albumin interactions with these surfaces. Specifically, we prepared a new PEG brush surface with a higher grafting density (PEG_{hg}, Fig. 3(a)) polyelectrolyte multilayers (PEM) made from polysaccharides (Fig. 3(b)), and two different glycocalyx mimetic surfaces consisting of PEM coated with GAG-rich polyelectrolyte complex nanoparticles (PCNs) with one of two different chemistries: chondroitin sulfate-chitosan (CS-CHI, Fig. 3(c)) or heparin-chitosan (HEP-CHI, Fig. 3(d)). All of these surfaces have been categorized as low-fouling or ultralow-fouling surfaces [16,39]. For all of these surfaces, the general trend of the surface protein density is similar; however, the irreversible aggregation occurs at very different times with different rates (see Fig. 3). The PEM surface, for example, shows a rapid transition from reversible adsorption of albumin to irreversible aggregation (after about 400 s), indicating that albumin (with 50 pM concentration in the solution) has a high affinity with the PEM such that protein aggregation occurs much faster in comparison to other surfaces. The aggregation occurs at a much later time for albumin adsorption on the glycocalyx mimetic and PEG_{hg} brush surfaces. Compared to the PEM, the glycocalyx mimetic surfaces extend the reversible adsorption and desorption by more than 20 times for both glycocalyx mimetic surfaces, and more than 10 times for PEG_{hg}. This indicates that although the glycocalyx mimetic surfaces and PEG_{hg} resist albumin accumulation on the surface, if we increase the time scale of the experiment, aggregation of the proteins on the surface is ultimately observed. Interestingly, this long-term aggregation behavior may not be observed on a PEG_{hg} if the experimental time were less than an hour, or on a PEM +PCN surface, if the experimental time is less than 3 h.

Both k_{ads} and k_{off} obtained from the short-time asymptotic behavior are summarized for each surface in Fig. 4. Most of the literature describing low-fouling and ultralow-fouling surfaces use this short-term behavior to qualify protein resistant materials. As Fig. 4(a) indicates, the albumin adsorption rate coefficient on the PEM surface is much higher than on the rest of the surfaces. The adsorption rate coefficient for albumin is reduced by more than two orders of magnitude for the glycocalyx mimetic and PEG brush surfaces compared to the PEM. This emphasizes the role of "bush-like" nanostructure of the PCNs in reducing the number of adsorbed albumin molecules, as we already reported in a short-term experiment [39].

For the PEM surface, although the adsorption rate coefficient is much higher than the other surfaces, the desorption rate coefficient of albumin is comparable to the other surfaces; confirming

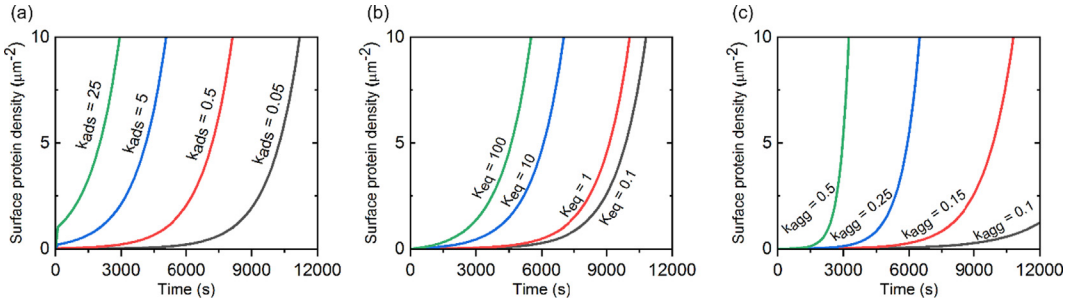

Fig. 2. Effect of individual parameters (rate coefficients or equilibrium constant) on macroscopic aggregation curves according to our mathematical model. (a) The onset of surface aggregation takes place more rapidly with increasing k_{ads} (s^{-1} μm^{-2} μM^{-1}). Note that for large k_{ads}, the protein density increases substantially at short times due to enhanced reversible adsorption. (b) Increasing K_{eq} (μm^{-2} μM^{-1}) leads to faster aggregation. (c) Increasing k_{agg} (s^{-1} μM^{-1}) leads to faster onset of aggregation. In all three panels, the concentration of protein is 0.005 μM and when changing either k_{ads}, K_{eq}, or k_{agg}, the rest of the parameters remained constant at k_{ads} = 0.1 s^{-1} μm^{-2} μM^{-1}, K_{eq} = 1 μm^{-2} μM^{-1}, and k_{agg} = 0.15 s^{-1} μM^{-1}.

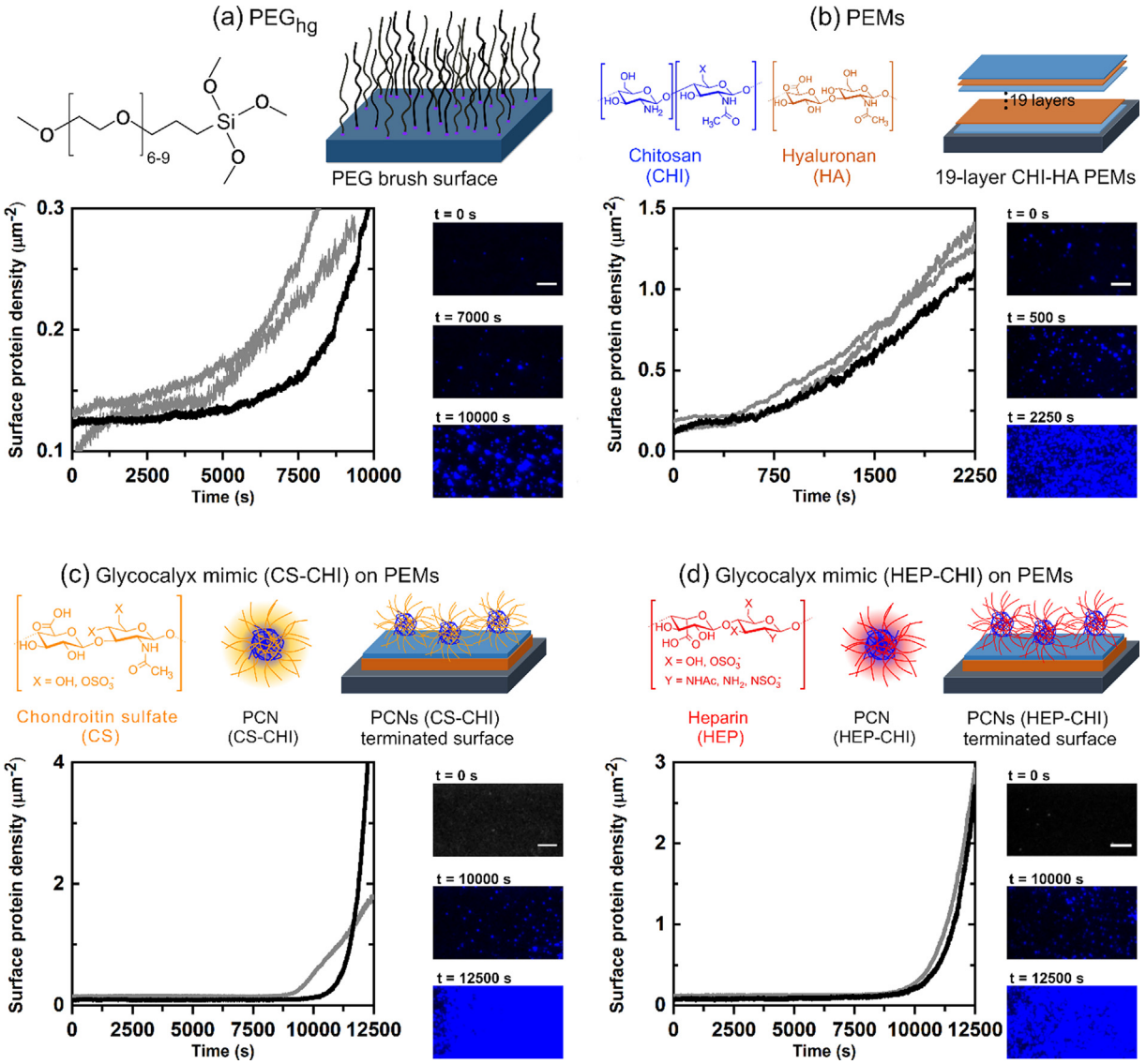

Fig. 3. (a) Chemical structure of the PEG-silane used to prepare PEG brush surfaces along with the sketch of the high grafting density PEG brush surface. BSA surface density on PEG_{hg} as a function of time is shown for three replicates together with representative TIRF images at three different times, scale bar = 5 μm. Fluorescent images are for the replicate curve shown in black. (b) Chemical structure of each polysaccharide used to prepare 19-layer PEM along with the sketch of the PEM surface. BSA surface density as a function of time is shown for three replicates. Representative TIRF images at three times for the replicate curve shown in black, scale bar = 5 μm (c) Chemical structure of the chondroitin sulfate and schematic of GAG-rich polyelectrolyte complex nanoparticles (PCNs), formed from CS and CHI that are adsorbed on the surface of the PEM as a mimic of the endothelial glycocalyx along with the sketch of the prepared surface. BSA surface density as a function of time is shown for two replicates. Representative TIRF images at three different times for the replicate curve shown in black, scale bar = 5 μm. (d) Chemical structure of the heparin and schematic of GAG-rich polyelectrolyte complex nanoparticles (PCNs), formed from HEP and CHI that are adsorbed on the surface of the PEM as another mimic of the endothelial glycocalyx along with the sketch of surface. BSA surface density as a function of time is shown for two replicates. Representative TIRF images at three different times for the replicate curve shown in black, scale bar = 5 μm.

that the adsorption of albumin molecules to the PEM is highly dynamic. In fact, the results confirm that the rate of desorption from the surface is very similar for all of the surfaces.

Further, we studied fibrinogen interactions with these surfaces in similar experiments with single-molecule microscopy. Fibrinogen exhibits a similar transition from reversible to irreversible adsorption, although the onset of accumulation and rates of irreversible adsorption are different than albumin for the same surfaces (see Fig. S1). The PEM surface, for example, is more resistant to fibrinogen than albumin, such that irreversible accumulation occurs after 2000 s of reversible adsorption and desorption. For the glycocalyx-mimetic surfaces made from HEP-CHI, the irreversible adsorption of fibrinogen occurs sooner than for the CS-CHI surface. This phenomenon is due to the specific binding between heparin and fibrinogen, which we have previously reported [39]. For PEG brush surfaces unlike the albumin, the onset of irreversible adsorption of fibrinogen occurs approximately at the same time for both PEG_{lg} and PEG_{hg}.

Note that this trend of protein interaction behavior is not limited to the concentration of the protein in the solution. For example, we performed similar experiments for the PEM and glycocalyx mimetic surface with HEP-CHI with lower and higher concentration of the protein, respectively (see Fig. S2). When the concentration of the albumin in the solution is reduced in half, we still observe similar behavior but with a longer period of time for the short-time, reversible adsorption phase, and obviously different rate of aggregation for the PEM. Similarly, for the glycocalyx mimetic surface, doubling the concentration of the fibrinogen in

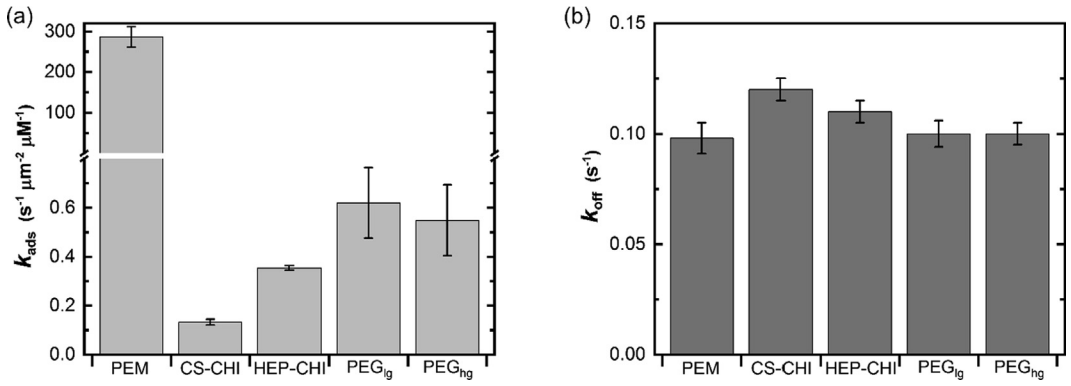

Fig. 4. (a) Adsorption rate coefficients and (b) desorption rate coefficients for BSA during the reversible adsorption for different surfaces studied in this work. Error bars represent the standard deviation (n = 3 independent experiments for each condition).

the solution results in faster onset of aggregation due to the concentration dependence of protein aggregation (see Fig. S2).

The results from dynamics of the protein interactions with low fouling and ultralow-fouling surfaces indicate that the type of both protein and surface affect the rate of protein adsorption and the time for the transition from the reversible to irreversible adsorption. In our experiments, the PEM has a high affinity for albumin, which is obvious from the adsorption rate coefficient and the short transition time. However, its affinity is lower for fibrinogen. For the PEM+PCNs (HEP-CHI) surface, we observe lower albumin adsorption rate coefficient and longer transition time than fibrinogen. Although, the rate of adsorption for both proteins is very similar for the PEM+PCNs (CS-CHI) surface, and is the lowest among all the surfaces. For PEG brush surfaces, the albumin adsorption rate coefficient is lower than fibrinogen. Furthermore, as the grafting density is increased, the adsorption rate coefficient of both proteins decreases. Our observed decrease in the adsorption rate coefficient with increasing grafting density is similar to what was observed in a previous study with fibronectin [27].

We further evaluated our proposed model with the experimental data obtained from albumin interaction with the other four surfaces presented above. Fig. 5 indicates that the proposed model can describe albumin interactions on different surfaces when we use the experimentally obtained k_{ads} and k_{off} parameters (from Fig. 4) measured directly from the single-molecule assay, and adjust the k_{agg} and K_{eq} parameters to match the experimental data. The other adjustable parameters are reported in Table S.2. The proposed model can also be used to describe the experimental data from fibrinogen interactions on different surfaces (see Fig. S4). Recall that the model predictions in Fig. 5 represent approximate solutions, in which desorption of higher oligomers is neglected, because this is not expected to occur at shorter times. However, for the PEM +PCN surfaces shown in Fig. 5(c) and (d), it is plausible that the model may match the data better if the desorption of higher oligomers (i < 3) were accounted for, as the time scale of these experiments is much longer.

The combined single-molecule experiments and kinetic analysis used here enable us to propose that protein interactions with nanostructured solid interfaces involve multiple steps. Understanding how proteins interact with interfaces, including kinetics of adsorption and desorption, and including possible conformational changes and aggregation are critical to design antifouling surfaces and investigating the behavior of protein interactions with solid interfaces. Our results suggest that designing antifouling surfaces based on short-term experiments with ensemble averaging methods may fail to inform about the long-term performance of non-fouling surfaces, because a reversible protein adsorption may persist for hours before accumulation is observed. Our long-term observations from two structurally different proteins with single-molecule microscopy reveal two regimes of behavior for protein interactions at interfaces. Reversible protein adsorption dominates the kinetics at early experimental times. This state is probed in short-term experiments that are frequently used to qualify protein adsorption on surfaces. However, by extending the experiments for a longer time, we observed irreversible protein adsorption that leads to protein aggregation on all of the surfaces studied in this work. The onset of accumulation occurs for all protein-surface pairs studied here, suggesting it is a general phenomenon, at least for the two important blood proteins, albumin and fibrinogen. Although the onset of accumulation occurred at different times and rates even for the same surface types. This implies the importance of long-term experiments when we study the behavior of protein interactions at interfaces. Our proposed model describes the adsorption and desorption of a distribution of oligomers formed in solution with low fouling surfaces. Based on our proposed model, new low-fouling or ultralow-fouling surface strategies should increase k_{off} and/or reduce k_{on}, k_{agg}, and K_{eq}. By targeting the phenomena governing these rates, new surfaces could be designed that extend the regime dominated by reversible adsorption, and that delay or even eliminate the transition to the aggregation-dominated regime.

4. Conclusions

This work demonstrates that surfaces conventionally defined as low- or ultralow protein fouling (*e.g.*, binding < 5 ng cm^{-2} of protein in a short-term adsorption experiment) accumulate adsorbed protein in long-term experiments. Single-molecule fluorescence microscopy was used to study the dynamics of protein molecules on various low- or ultralow-fouling surfaces to investigate long-term protein interactions.

Previous theoretical models of protein adsorption have been developed based on ensemble-averaging methods [54,55], and short-term experiments [56,29]. There are several differences between our model and other previous models. Our model introduces an irreversible surface-mediated protein aggregation step that correctly captures observed behavior, and can predict protein accumulation on surfaces, even when this adsorption is only seen at very long experimental times. This model is validated through single-molecule localization microscopy. Contrary to the models developed based on surface plasmon resonance (SPR), quartz crystal microbalance (QCM), or circular dichroism (CD), our experiments enable observation of single protein molecules and measure different rates of adsorption and desorption. Furthermore, while prior experimental observations have confirmed short-term reversibility and long-term protein accumulation, the studies

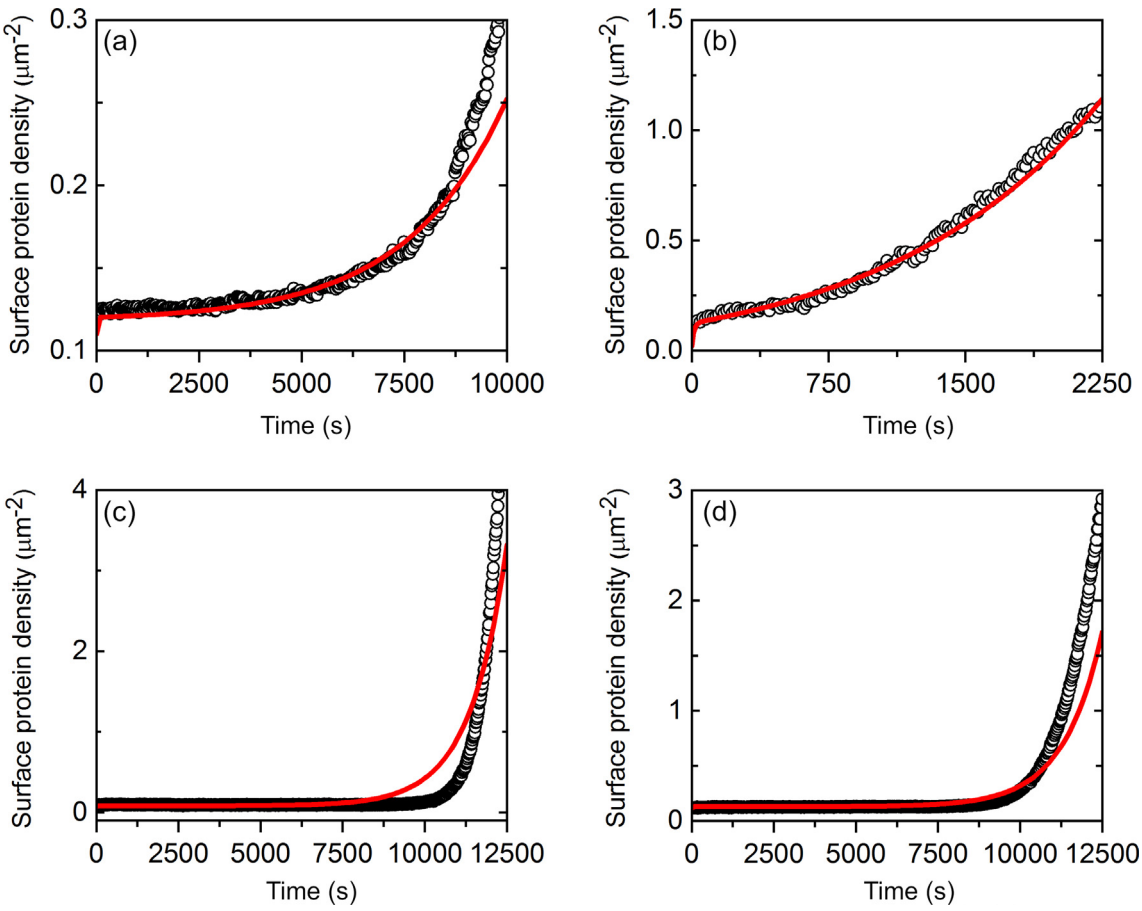

Fig. 5. Comparison of proposed model (surface-induced aggregation of protein oligomers) with experimental data from each of four different surfaces. Circles represent data from single-molecule TIRF microscopy for BSA on (a) PEG_{hg}, (b) PEM, (c) PEM+PCNs (CS-CHI) and (d) PEM+PCNs (HEP-CHI). Solid red lines represent the model. (For interpretation of the references to colour in this figure legend, the reader is referred to the web version of this article.)

conducted here bridge the gap between these two experimental time scales. Including the long-term behavior of the protein molecules in our model makes the model more generally applicable to real-world applications.

Our model enables prediction of two asymptotic behaviors: at short time, reversible adsorption and desorption dominate the kinetics, whereas at longer times, protein adsorption kinetics are governed by irreversible aggregation leading to rapid accumulation of protein on the surfaces. This model correctly predicts protein aggregation on low-fouling materials with different surface physical chemistry, through introduction of a surface-induced aggregation mechanism. The model also shows that achieving very low protein adsorption in short-term experiments is insufficient to prevent protein accumulation for long-term exposure. Instead, protein stability (*i.e.*, reduced aggregation), preferential adsorption of specific beneficial protein layers to regulate biological responses, and the use of other dynamic processes (*e.g.*, fluid shear) may ultimately be required to develop non-fouling surfaces that prevent blood coagulation, biofilm formation, inflammation, and other protein-mediated biological responses to materials. We envision that the experimental results shown here and the model we have proposed will lead others to reconsider the criteria for design and qualification of low-fouling and ultralow-fouling surfaces. Future strategies for improving low-fouling surfaces, should include evaluation of long-term (>1000 s) protein-surface interactions, reducing irreversible surface-induced aggregation, and stabilizing the native conformation of reversibly-bound or weakly-interacting proteins, so that they can desorb, rather than denature. Further extensions of this model should also include multi-protein-surface interaction mechanisms that could expand the scope and applicability of this work.

5. Data availability

The processed data required to reproduce these findings are available to download from data.mendeley.com.

CRediT authorship contribution statement

Mohammadhasan Hedayati: Conceptualization, Methodology, Validation, Investigation, Formal analysis, Writing - review & editing. **Diego Krapf:** Conceptualization, Methodology, Validation, Supervision, Writing - review & editing, Funding acquisition. **Matt J. Kipper:** Conceptualization, Validation, Resources, Supervision, Project administration, Funding acquisition.

Declaration of Competing Interest

The authors declare that they have no known competing financial interests or personal relationships that could have appeared to influence the work reported in this paper.

Acknowledgements

This work was supported by the National Science Foundation (award numbers 1511830 and 1531921).

Appendix A. Supplementary material

Supplementary data to this article can be found online at https://doi.org/10.1016/j.jcis.2021.01.001.

References

[1] M. Hedayati, M.J. Neufeld, M.M. Reynolds, M.J. Kipper, The quest for blood-compatible materials: recent advances and future technologies, Mater. Sci. Eng. R Rep. 138 (2019) 118–152, https://doi.org/10.1016/j.mser.2019.06.002.

[2] Q. Xie, J. Pan, C. Ma, G. Zhang, Dynamic surface antifouling: mechanism and systems, Soft Matter. 15 (2019) 1087–1107, https://doi.org/10.1039/C8SM01853G.

[3] N. Liu, Z. Xu, A. Morrin, X. Luo, Low fouling strategies for electrochemical biosensors targeting disease biomarkers, Anal. Methods. 11 (2019) 702–711, https://doi.org/10.1039/C8AY02674B.

[4] Z. Zhang, M. Zhang, S. Chen, T.A. Horbett, B.D. Ratner, S. Jiang, Blood compatibility of surfaces with superlow protein adsorption, Biomaterials 29 (2008) 4285–4291, https://doi.org/10.1016/j.biomaterials.2008.07.039.

[5] Q. Wei, T. Becherer, S. Angioletti-Uberti, J. Dzubiella, C. Wischke, A.T. Neffe, A. Lendlein, M. Ballauff, R. Haag, Protein interactions with polymer coatings and biomaterials, Angew. Chem. Int. Ed. 53 (2014) 8004–8031, https://doi.org/10.1002/anie.201400546.

[6] M. Rabe, D. Verdes, S. Seeger, Understanding protein adsorption phenomena at solid surfaces, Adv. Colloid Interface Sci. 162 (2011) 87–106, https://doi.org/10.1016/j.cis.2010.12.007.

[7] B.K.D. Ngo, M.A. Grunlan, Protein resistant polymeric biomaterials, ACS Macro Lett. 6 (2017) 992–1000, https://doi.org/10.1021/acsmacrolett.7b00448.

[8] I. Firkowska-Boden, X. Zhang, K.D. Jandt, Controlling protein adsorption through nanostructured polymeric surfaces, Adv. Healthc. Mater. 7 (2018) 1700995, https://doi.org/10.1002/adhm.201700995.

[9] E. Migliorini, M. Weidenhaupt, C. Picart, Practical guide to characterize biomolecule adsorption on solid surfaces (Review), Biointerphases. 13 (2018) 06D303, https://doi.org/10.1116/1.5045122.

[10] P.K. Thalla, H. Fadlallah, B. Liberelle, P. Lequoy, G. De Crescenzo, Y. Merhi, S. Lerouge, Chondroitin sulfate coatings display low platelet but high endothelial cell adhesive properties favorable for vascular implants, Biomacromolecules. 15 (2014) 2512–2520, https://doi.org/10.1021/bm5003762.

[11] G. Emilsson, R.L. Schoch, L. Feuz, F. Höök, R.Y.H. Lim, A.B. Dahlin, Strongly stretched protein resistant poly(ethylene glycol) brushes prepared by grafting-to, ACS Appl. Mater. Interfaces. 7 (2015) 7505–7515, https://doi.org/10.1021/acsami.5b01590.

[12] Y. Wei, H.-C. Hung, F. Sun, T. Bai, P. Zhang, A.K. Nowinski, S. Jiang, Achieving low-fouling surfaces with oppositely charged polysaccharides via LBL assembly, Acta Biomater. 40 (2016) 16–22, https://doi.org/10.1016/j.actbio.2016.04.013.

[13] B. Xu, C. Feng, J. Hu, P. Shi, G. Gu, L. Wang, X. Huang, Spin-casting polymer brush films for stimuli-responsive and anti-fouling surfaces, ACS Appl. Mater. Interfaces. 8 (2016) 6685–6692, https://doi.org/10.1021/acsami.5b12820.

[14] D. Hong, H.-C. Hung, K. Wu, X. Lin, F. Sun, P. Zhang, S. Liu, K.E. Cook, S. Jiang, Achieving ultralow fouling under ambient conditions via surface-initiated ARGET ATRP of carboxybetaine, ACS Appl. Mater. Interfaces. 9 (2017) 9255–9259, https://doi.org/10.1021/acsami.7b01530.

[15] C. Zhang, J. Yuan, J. Lu, Y. Hou, W. Xiong, H. Lu, From neutral to zwitterionic poly(α-amino acid) nonfouling surfaces: effects of helical conformation and anchoring orientation, Biomaterials. 178 (2018) 728–737, https://doi.org/10.1016/j.biomaterials.2018.01.052.

[16] M. Hedayati, D.F. Marruecos, D. Krapf, J.L. Kaar, M.J. Kipper, Protein adsorption measurements on low fouling and ultralow fouling surfaces: A critical comparison of surface characterization techniques, Acta Biomater. 102 (2020) 169–180, https://doi.org/10.1016/j.actbio.2019.11.019.

[17] W. Yu, J. Koc, J.A. Finlay, J.L. Clarke, A.S. Clare, A. Rosenhahn, Layer-by-layer constructed hyaluronic acid/chitosan multilayers as antifouling and fouling-release coatings, Biointerphases. 14 (2019), https://doi.org/10.1116/1.5110887 051002.

[18] X. Liu, L. Yuan, D. Li, Z. Tang, Y. Wang, G. Chen, H. Chen, J.L. Brash, Blood compatible materials: state of the art, J. Mater. Chem. B. 2 (2014) 5718–5738.

[19] Y. Chen, B. Pidhatika, T. von Erlach, R. Konradi, M. Textor, H. Hall, T. Lühmann, Comparative assessment of the stability of nonfouling poly(2-methyl-2-oxazoline) and poly(ethylene glycol) surface films: An *in vitro* cell culture study, Biointerphases. 9 (2014), https://doi.org/10.1116/1.4878461 031003.

[20] J. Ulbricht, R. Jordan, R. Luxenhofer, On the biodegradability of polyethylene glycol, polypeptoids and poly(2-oxazoline)s, Biomaterials. 35 (2014) 4848–4861, https://doi.org/10.1016/j.biomaterials.2014.02.029.

[21] G. Cheng, G. Li, H. Xue, S. Chen, J.D. Bryers, S. Jiang, Zwitterionic carboxybetaine polymer surfaces and their resistance to long-term biofilm formation, Biomaterials. 30 (2009) 5234–5240, https://doi.org/10.1016/j.biomaterials.2009.05.058.

[22] R. Walder, M. Kastantin, D.K. Schwartz, High throughput single molecule tracking for analysis of rare populations and events, The Analyst. 137 (2012) 2987, https://doi.org/10.1039/c2an16219a.

[23] H. Shen, L.J. Tauzin, R. Baiyasi, W. Wang, N. Moringo, B. Shuang, C.F. Landes, Single particle tracking: from theory to biophysical applications, Chem. Rev. 117 (2017) 7331–7376, https://doi.org/10.1021/acs.chemrev.6b00815.

[24] M. Hedayati, M.J. Kipper, D. Krapf, Anomalous protein kinetics on low-fouling surfaces, Phys. Chem. Chem. Phys. 22 (2020) 5264–5271, https://doi.org/10.1039/D0CP00326C.

[25] M. Kastantin, B.B. Langdon, E.L. Chang, D.K. Schwartz, Single-molecule resolution of interfacial fibrinogen behavior: effects of oligomer populations and surface chemistry, J. Am. Chem. Soc. 133 (2011) 4975–4983, https://doi.org/10.1021/ja110663u.

[26] D. Wang, C. He, M.P. Stoykovich, D.K. Schwartz, Nanoscale topography influences polymer surface diffusion, ACS Nano. 9 (2015) 1656–1664, https://doi.org/10.1021/nn506376n.

[27] D. Faulón Marruecos, M. Kastantin, D.K. Schwartz, J.L. Kaar, Dense poly (ethylene glycol) brushes reduce adsorption and stabilize the unfolded conformation of fibronectin, Biomacromolecules. 17 (2016) 1017–1025, https://doi.org/10.1021/acs.biomac.5b01657.

[28] D. Faulón Marruecos, D.F. Kienle, J.L. Kaar, D.K. Schwartz, Grafting density impacts local nanoscale hydrophobicity in poly(ethylene glycol) brushes, ACS Macro Lett. 7 (2018) 498–503, https://doi.org/10.1021/acsmacrolett.8b00004.

[29] K. Wang, Y. Chen, X. Gong, J. Xia, J. Zhao, L. Shen, A mobile precursor determines protein resistance on nanostructured surfaces, Phys. Chem. Chem. Phys. 20 (2018) 12527–12534, https://doi.org/10.1039/C8CP00887F.

[30] H. Shen, L.J. Tauzin, W. Wang, B. Hoener, B. Shuang, L. Kisley, A. Hoggard, C.F. Landes, Single-molecule kinetics of protein adsorption on thin nylon-6,6 films, Anal. Chem. 88 (2016) 9926–9933, https://doi.org/10.1021/acs.analchem.5b04081.

[31] M. Armstrong, H. Hess, S. Tsitkov, Statistical inference in single molecule measurements of protein adsorption, in: A.N. Cartwright, D.V. Nicolau, D. Fixler (Eds.), Nanoscale Imaging Sens. Actuation Biomed. Appl. XV, SPIE, San Francisco, United States, 2018: p. 46. https://doi.org/10.1117/12.2290918.

[32] C.F. Wertz, M.M. Santore, Effect of surface hydrophobicity on adsorption and relaxation kinetics of albumin and fibrinogen: single-species and competitive behavior, Langmuir. 17 (2001) 3006–3016, https://doi.org/10.1021/la0017781.

[33] J. Kim, Mathematical modeling approaches to describe the dynamics of protein adsorption at solid interfaces, Colloids Surf. B Biointerfaces. 162 (2018) 370–379, https://doi.org/10.1016/j.colsurfb.2017.12.006.

[34] Z. Adamczyk, Protein adsorption: a quest for a universal mechanism, Curr. Opin. Colloid Interface Sci. 41 (2019) 50–65, https://doi.org/10.1016/j.cocis.2018.11.004.

[35] Z. Adamczyk, A. Pomorska, M. Nattich-Rak, M. Wytrwal-Sarna, A. Bernasik, Protein adsorption mechanisms at rough surfaces: Serum albumin at a gold substrate, J. Colloid Interface Sci. 530 (2018) 631–641, https://doi.org/10.1016/j.jcis.2018.06.063.

[36] R.A. Latour, The langmuir isotherm: a commonly applied but misleading approach for the analysis of protein adsorption behavior: protein adsorption and the langmuir isotherm, J. Biomed. Mater. Res. A. 103 (2015) 949–958, https://doi.org/10.1002/jbm.a.35235.

[37] E.L. Hinrichsen, J. Feder, T. Jøssang, Geometry of random sequential adsorption, J. Stat. Phys. 44 (1986) 793–827, https://doi.org/10.1007/BF01011908.

[38] D. Krapf, R. Metzler, Strange interfacial molecular dynamics, Phys. Today. 72 (2019) 48–54, https://doi.org/10.1063/PT.3.4294.

[39] M. Hedayati, M.M. Reynolds, D. Krapf, M.J. Kipper, Nanostructured surfaces that mimic the vascular endothelial glycocalyx reduce blood protein adsorption and prevent fibrin network formation, ACS Appl. Mater. Interfaces. 10 (2018) 31892–31902, https://doi.org/10.1021/acsami.8b09435.

[40] S.S. Shah, J.Y. Lee, S. Verkhoturov, N. Tuleuova, E.A. Schweikert, E. Ramanculov, A. Revzin, Exercising Spatiotemporal control of cell attachment with optically transparent microelectrodes, Langmuir. 24 (2008) 6837–6844, https://doi.org/10.1021/la800231e.

[41] T.J. Plegue, K.M. Kovach, A.J. Thompson, J.A. Potkay, Stability of polyethylene glycol and zwitterionic surface modifications in PDMS microfluidic flow chambers, Langmuir. 34 (2018) 492–502, https://doi.org/10.1021/acs.langmuir.7b03095.

[42] P.C.F. da Câmara, R.C. Balaban, M. Hedayati, K.C. Popat, A.F. Martins, M.J. Kipper, Novel cationic tannin/glycosaminoglycan-based polyelectrolyte multilayers promote stem cells adhesion and proliferation, RSC Adv. 9 (2019) 25836–25846, https://doi.org/10.1039/C9RA03903A.

[43] A.F. Martins, J. Vlcek, T. Wigmosta, M. Hedayati, M.M. Reynolds, K.C. Popat, M.J. Kipper, Chitosan/iota-carrageenan and chitosan/pectin polyelectrolyte multilayer scaffolds with antiadhesive and bactericidal properties, Appl. Surf. Sci. 502 (2020), https://doi.org/10.1016/j.apsusc.2019.144282 144282.

[44] M. Hedayati, M.J. Kipper, Atomic force microscopy of adsorbed proteoglycan mimetic nanoparticles: toward new glycocalyx-mimetic model surfaces, Carbohydr. Polym. 190 (2018) 346–355, https://doi.org/10.1016/j.carbpol.2018.02.023.

[45] S. Boddohi, N. Moore, P.A. Johnson, M.J. Kipper, Polysaccharide-based polyelectrolyte complex nanoparticles from chitosan, heparin, and hyaluronan, Biomacromolecules. 10 (2009) 1402–1409.

[46] G. Campagnola, K. Nepal, B.W. Schroder, O.B. Peersen, D. Krapf, Superdiffusive motion of membrane-targeting C2 domains, Sci. Rep. 5 (2015), https://doi.org/10.1038/srep17721.

[47] M.G. Gervasi, X. Xu, B. Carbajal-Gonzalez, M.G. Buffone, P.E. Visconti, D. Krapf, The actin cytoskeleton of the mouse sperm flagellum is organized in a helical structure, J. Cell Sci. 131 (2018) jcs215897, https://doi.org/10.1242/jcs.215897.

[48] R.E. Benesch, R. Benesch, Enzymatic removal of oxygen for polarography and related methods, Science. 118 (1953) 447–448, https://doi.org/10.1126/science.118.3068.447.

[49] K. Jaqaman, D. Loerke, M. Mettlen, H. Kuwata, S. Grinstein, S.L. Schmid, G. Danuser, Robust single-particle tracking in live-cell time-lapse sequences, Nat. Methods. 5 (2008) 695–702, https://doi.org/10.1038/nmeth.1237.
[50] E. Hellstrand, B. Boland, D.M. Walsh, S. Linse, Amyloid β-protein aggregation produces highly reproducible kinetic data and occurs by a two-phase process, ACS Chem. Neurosci. 1 (2010) 13–18, https://doi.org/10.1021/cn900015v.
[51] P. Arosio, T.P.J. Knowles, S. Linse, On the lag phase in amyloid fibril formation, Phys. Chem. Chem. Phys. 17 (2015) 7606–7618, https://doi.org/10.1039/C4CP05563B.
[52] M. Törnquist, T.C.T. Michaels, K. Sanagavarapu, X. Yang, G. Meisl, S.I.A. Cohen, T.P.J. Knowles, S. Linse, Secondary nucleation in amyloid formation, Chem. Commun. 54 (2018) 8667–8684, https://doi.org/10.1039/C8CC02204F.
[53] C. Li, L. Xu, Y.Y. Zuo, P. Yang, Tuning protein assembly pathways through superfast amyloid-like aggregation, Biomater. Sci. 6 (2018) 836–841, https://doi.org/10.1039/C8BM00066B.
[54] L.M. Pandey, S.K. Pattanayek, D. Delabouglise, Properties of adsorbed bovine serum albumin and fibrinogen on self-assembled monolayers, J. Phys. Chem. C. 117 (2013) 6151–6160, https://doi.org/10.1021/jp309483p.
[55] M.P. Schmidt, C.E. Martínez, Kinetic and conformational insights of protein adsorption onto montmorillonite revealed using in situ ATR-FTIR/2D-COS, Langmuir. 32 (2016) 7719–7729, https://doi.org/10.1021/acs.langmuir.6b00786.
[56] C.F. Wertz, M.M. Santore, Fibrinogen adsorption on hydrophilic and hydrophobic surfaces: geometrical and energetic aspects of interfacial relaxations, Langmuir. 18 (2002) 706–715, https://doi.org/10.1021/la011075z.